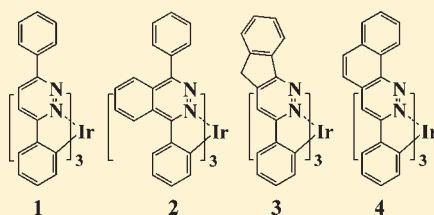


First-Principles Studies on the Efficient Photoluminescent Iridium(III) Complexes with C[^]N=N LigandsLili Shi,[†] Juanjuan Su,^{†,‡} and Zhijian Wu^{*,†}[†]State Key Laboratory of Rare Earth Resource Utilization, Changchun Institute of Applied Chemistry, Chinese Academy of Sciences, Changchun 130022, People's Republic of China[‡]Graduate School, Chinese Academy of Sciences, Beijing 100049, People's Republic of China

Supporting Information

ABSTRACT: The electronic structures and photophysical properties of several homoleptic iridium complexes IrL₃ with C[^]N=N ligands, including **1** (L = 3,6-diphenylpyridazine), **2** (L = 1,4-diphenylphthalazine), **3** (L = 3-phenyl-5H-indeno[1,2-*c*]pyridazine), and **4** (L = 3-phenylbenzo[*h*]cinnoline), are investigated using the density functional method. The comparison between the calculated results of the four complexes shows that the assumed complex **4** may possess higher photoluminescent quantum efficiency than complexes **1–3** and is the potential candidate to be an efficient green-emitting material. The photophysical properties of the assumed complex **3** can be comparable to that of experimentally found complex **1**. For **1** and **3**, the emission energies are nearly the same, consistent with their similar HOMO–LUMO energy gaps. Their emission characters are also similar and mainly dominated by one ligand. For **4** and the experimentally found complex **2**, although they have similar HOMO–LUMO energy gaps, and their luminescent nature is nearly the same and dominated by the three ligands, the emission spectrum of **4** is blue-shifted as compared to that of **2**.



1. INTRODUCTION

Phosphorescent transition-metal complexes have attracted great attention in the development of highly efficient organic light-emitting diode (OLED).^{1–4} The phosphors can harvest both the singlet and the triplet excitons as light, resulting in a theoretical level of unity for internal quantum efficiency in phosphorescent OLEDs.^{5,6} Among the transition-metal complexes reported, cyclometalated iridium(III) complexes are the most promising candidates^{2,7,8} because of their high thermal stability and short lifetime in excited states, which could reduce the probabilities of triplet–triplet annihilation^{4,9–11} and increase photoluminescent (PL) quantum efficiencies.

The photophysical properties of cyclometalated Ir(III) complexes mainly depend on the character and energy level of frontier molecular orbitals (FMO), especially HOMO (highest occupied molecular orbital) and LUMO (lowest unoccupied molecular orbital), which are governed by the basic skeletal arrangement of both the chromophoric and/or the ancillary ligands.¹² The majority of cyclometalated Ir(III) complexes are heteroleptic complexes, such as (C[^]N)₂Ir(acac), where acac represents acetylacetonate.^{4,13,14} Reports on highly emissive homoleptic Ir(III) complexes are still rare, because high temperatures are required for their syntheses. Thus, the majority of the homoleptic cyclometalated chelates cannot withstand such stringent reaction conditions and lead to severe decomposition.^{6,15} Recently, a new class of homoleptic Ir(III) complexes with C[^]N=N structure as ligands (**1** and **2** in Figure 1) is reported and proved to be strong phosphorescent materials with good thermal stabilities.^{16–18} The

stable tris-cyclometalated form has been regarded as partially originating from the small steric hindrance in the C[^]N=N type ligand (no other atoms attach to N atoms adjacent to the chelating N atoms).

From the experimental molecular structures of **1** and **2**, it can be seen that the nonchelating phenyl in the ligands is flexible. In this study, we propose two additional artificial structures (**3** and **4** in Figure 1) in which the rotation of the flexible phenyl group has been restricted. The four molecules shown in Figure 1 have been studied in this Article by using the density functional theory (DFT). Physical properties, such as the electronic structures, charge injection, and transport, and spectral properties of the four complexes have been calculated and compared to the available experimental data. PL quantum efficiencies are also discussed on the basis of the calculated results.

2. COMPUTATIONAL METHODS

The ground-state geometry for each molecule was optimized by using the density functional theory. Vibrational frequencies were calculated at the same theoretical level to confirm that each configuration was a minimum on the potential energy surface. All open-shell calculations were performed with unrestricted methods, and spin contamination in the radical species can be neglected. Becke's three-parameter hybrid method¹⁹ combining with the Lee–Yang–Parr correlation functional²⁰ (denoted as B3LYP) was adopted here. The geometry optimizations of

Received: December 22, 2010

Published: May 20, 2011

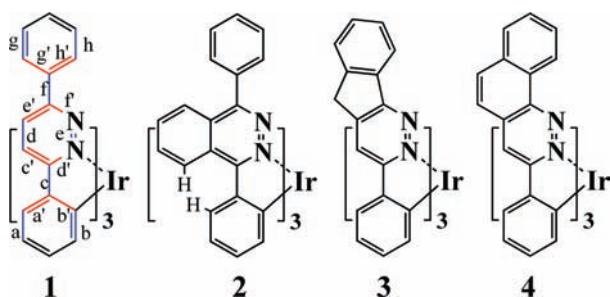


Figure 1. The schematic structures for the studied complexes.

the lowest triplet states (T_1) were performed by unrestricted B3LYP approach. On the basis of the ground- and excited-state equilibrium geometries, the time-dependent DFT (TD-DFT) approach associated with the polarized continuum model (PCM) in dichloromethane (CH_2Cl_2) media was applied to investigate the absorption and emission spectral properties.

The “double- ξ ” quality basis set LANL2DZ^{21,22} associated with the pseudopotential was employed on atom Ir. The 6-31G(d) basis set was used for nonmetal atoms in the gradient optimizations. Recent calculations with the above-mentioned methods and basis sets for transition-metal complexes have supported their reliability and gave good agreement with experimental results.^{23–25} In fact, many studies have shown that theoretical work becomes more important in both elucidating and predicting the chemical and physical properties of the complexes. No symmetry constraint was used during the geometry optimizations for the studied complexes. All calculations were performed with the Gaussian 03 software package.²⁶

3. RESULTS AND DISCUSSION

3.1. Molecular Geometries in the Ground and Lowest Triplet States. The schematic structures of the studied complexes 1–4 and the representative optimized structure of 2 in the ground state (S_0) at B3LYP level are shown in Figures 1 and 2, respectively. The stable isomers of these studied complexes adopt configurations with the chelating phenyl fragments at the cis location (as can be seen for 2 in Figure 2).²⁷ Ir(III) with d^6 configuration adopts a pseudo-octahedral coordination geometry.

The optimized geometry parameters of 1–4 in the ground and lowest triplet states (T_1) together with the available X-ray crystallography data¹⁷ of 2 are shown in Table 1. Figure 2 gives the bond labels (Ir–C1, Ir–N1, $d_1(\text{A})$, $d_2(\text{A})$, $d_1(\text{B})$, $d_2(\text{B})$, etc.), which are used in Table 1. The optimized bond distances of 2 agree well with the experimental data, and the deviation is within 3%. Table 1 also shows that changes of the ligands have little influence on the metal–ligand (Ir–C and Ir–N) bond distances. For the assumed complexes 3 and 4, their corresponding ligands are nearly coplanar because the dihedral angles C2–C4–C5–N2 and N4–C6–C7–C8 are close to 0° , indicating that they possess rigid skeletal structures, which may effectively prevent the nonradiative decay. For 2, due to the repulsion interaction of the two H atoms localized on the chelating phenyl part and N=N moiety (see Figure 1), the dihedral angle C2–C4–C5–N2 is 13.3° larger than that of the other complexes, leading to its slightly longer d_1 (1.465 Å). The dihedral angles N4–C6–C7–C8 of 1 and 2 are 22.2° and 40.4° , respectively. The large dihedral angles result in the poor conjugated degree between peripheral phenyl ring and N=N moiety and longer d_2 values for 1 and 2.

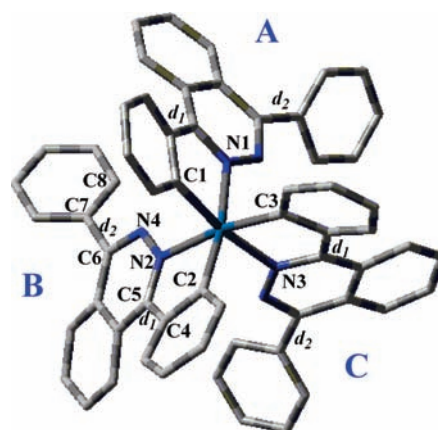


Figure 2. Representative optimized structure of 2 in the ground state at the B3LYP level.

From S_0 to T_1 states, the bond distances of Ir–C3, Ir–N3, $d_1(\text{C})$, $d_2(\text{C})$ in 1 and Ir–C1, Ir–N1, $d_1(\text{A})$, $d_2(\text{A})$ in 3 are shortened significantly. The bond distance change of 1 and 3 mainly occurs in one of the ligands, that is, ligand C for 1 and ligand A for 3. The shortened Ir–C3, Ir–N3 in 1 and Ir–C1, Ir–N1 in 3 will strengthen the interaction of iridium with the ligand C of 1 and ligand A of 3. This might increase the probability of charge transfer from metal to ligand C in 1 and ligand A in 3. The little change of the bond distances in 2 and 4 suggests that the characters of their lowest triplet excited states would be influenced by the three ligands. These points are confirmed by bond length alternation (BLA) in the following.

To clarify the geometry relaxation from S_0 to T_1 on three ligands, we employ the concept of BLA, which is the difference between the average bond distance of the “single” and “double” bonds.²⁸ The degree of BLA has been used as a structural parameter in interpreting electronic spectra of many classes of conjugated molecules.²⁹ Herein, BLA is defined by the formula:

$$\text{BLA} = (a' + b' + c' + d' + e' + f' + g' + h')/8 - (a + b + c + d + e + f + g + h)/8$$

where the labels a , a' , etc., are bond distances as schematic in 1 of Figure 1. Table 2 lists the BLA values in S_0 and T_1 states and their differences ($\Delta\text{BLA}(T_1-S_0)$) for the three ligands in the studied complexes. The $\Delta\text{BLA}(T_1-S_0)$ values show that only ligand C in 1 and ligand A in 3 undergo the obvious geometry relaxation from S_0 to T_1 , which might also be an indication that their phosphorescent characters could be dominated by that ligand with the changed bond distance. The $\Delta\text{BLA}(T_1-S_0)$ values for 2 and 4 reveal that the charge transfer would happen on the three ligands. Moreover, the $\Delta\text{BLA}(T_1-S_0)$ value of 3 (0.041 Å) is slightly smaller than that of 1 (0.043 Å), indicating that the geometry relaxation of 3 from T_1 to S_0 is less than that of 1. More importantly, the smallest absolute $\Delta\text{BLA}(T_1-S_0)$ values in 4 indicate that it has the smallest geometry relaxation among the studied complexes, which could reduce the nonradiative decay and enhance PL quantum efficiency.

3.2. Electronic Structures of the Ligands and the Complexes. The contour plots of HOMO and LUMO and their energies for ligands 1L–4L (1L represents the ligands in complex 1; the same applies to 2L, 3L, and 4L) and for the whole complexes 1–4 are shown in Figure 3a and b, respectively. Because of the similar π -conjugated extension, the HOMO–LUMO energy

Table 1. Main Optimized Geometry Parameters for 1–4 Together with the Experimental Data of 2^a

	1		2		3		4		exp. ¹⁷
	S ₀	T ₁	S ₀	T ₁	S ₀	T ₁	S ₀	T ₁	
Bond Length/Å									
Ir–C1	2.032	2.046	2.027	2.016	2.031	2.002	2.033	2.022	2.019
Ir–C2	2.032	2.026	2.028	2.013	2.029	2.048	2.033	2.023	2.021
Ir–C3	2.032	1.997	2.029	2.021	2.031	2.023	2.033	2.022	2.017
Ir–N1	2.150	2.170	2.153	2.154	2.151	2.097	2.147	2.151	2.102
Ir–N2	2.150	2.172	2.152	2.144	2.150	2.178	2.147	2.150	2.095
Ir–N3	2.150	2.117	2.152	2.152	2.151	2.170	2.147	2.151	2.089
d ₁ (A)	1.460	1.462	1.465	1.458	1.463	1.411	1.463	1.467	
d ₁ (B)		1.461		1.454		1.465			
d ₁ (C)		1.411		1.458		1.464			
d ₂ (A)	1.484	1.483	1.488	1.484	1.465	1.445	1.453	1.453	
d ₂ (B)		1.482		1.483		1.464			
d ₂ (C)		1.459		1.484		1.465			
Bond Angle/deg									
C1–Ir–N1	79.0	78.8	78.1	78.4	79.0	81.1	79.2	79.1	
C2–Ir–N1	171.6	171.4	170.3	171.4	172.0	171.9	172.3	171.7	
N1–Ir–N2	94.5	93.3	94.0	93.0	94.7	93.9	94.8	92.8	
Dihedral Angle/deg									
C2–C4–C5–N2	1.2	1.4	13.3	13.8	1.0	0.5	0.6	3.7	
N4–C6–C7–C8	22.2	25.7	40.4	37.3	0.4	0.3	0.5	0.8	

^a For bond labels Ir–C1, Ir–N1, d₁(A), d₂(A), etc., see Figure 2.

Table 2. Calculated Bond Length Alternation (BLA, Å) in S₀ and T₁ States and Their Difference (ΔBLA(T₁–S₀)) for Three Ligands in the Studied Complexes

	BLA(S ₀)	BLA(T ₁)	ΔBLA(T ₁ –S ₀)
1(A)	–0.008	–0.008	0
1(B)	–0.008	–0.008	0
1(C)	–0.008	0.036	0.043
2(A)	–0.014	–0.007	0.006
2(B)	–0.014	0.001	0.014
2(C)	–0.014	–0.007	0.007
3(A)	–0.007	0.034	0.041
3(B)	–0.007	–0.007	0
3(C)	–0.007	–0.007	0
4(A)	–0.002	–0.007	–0.005
4(B)	–0.002	–0.007	–0.005
4(C)	–0.002	–0.007	–0.005

gaps of rigid ligands 3L (4.53 eV) and 4L (4.24 eV) are similar to flexible ones 1L (4.51 eV) and 2L (4.22 eV), respectively. Thus, we hope that the emission energies of 3 and 4 are similar to those of 1 and 2, respectively, and using 3L and 4L instead of 1L and 2L to increase the PL quantum efficiency is feasible. In fact, complexes 1 and 2 indeed have energy gaps similar to those of 3 and 4, respectively (see Figure 3b).

Figure 3b shows that the HOMOs of the studied complexes are localized on 5d(Ir) (>45%) and the three chelating phenyl moieties. The LUMO spatial distribution of 1–4 is similar to that of the corresponding ligands 1L–4L shown in Figure 3a, which is

mainly contributed by the N=N moieties. The trend of LUMO energy levels for the complexes and their corresponding ligands is the same, that is, 4 (4L) < 2 (2L) < 1 (1L) < 3 (3L). This is also true for the HOMO energy levels between the complexes and their corresponding ligands. This means that the selected ligands are very important because their HOMO and LUMO energy levels are closely related to the HOMO and LUMO energy levels of the complexes and will influence the emission spectra significantly.

3.3. Absorption Spectra in CH₂Cl₂ Media. The absorption energies, oscillator strengths (*f*), dominant configurations, and transition nature of the selected excited states with *f* > 0.06 are listed in Table 3. It can be seen that the calculated results agree well with the experimental data.^{16,17} Simulated UV–visible absorption spectra (Figure 4) of 1–4 in CH₂Cl₂ media show that 1, 3, and 4 have similar absorption curves in band locations. In comparison with 1, 3, and 4, the absorption spectra of 2 are red-shifted.

The lowest allowed transitions are located at 449 nm (*f* = 0.020) for 1, 534 nm (*f* = 0.030) for 2, 437 nm (*f* = 0.081) for 3, and 501 nm (*f* = 0.012) for 4. These transitions are attributed to MLCT (metal to ligand charge transfer)/ILCT (intraligand charge transfer) characters [d(Ir) + π(phenyl) → π*(N=N moiety)]. The large π-conjugated extension and small energy gaps of ligands 2L and 4L result in the red-shift of their corresponding complexes 2 and 4. Complexes 1, 3, and 4 have absorptions around 300 and 400 nm, which are characterized as MLCT/ILCT and MLCT/ILCT/LLCT (LLCT refers to the ligand to ligand charge transfer), respectively. The weak absorption at 476 nm for 4 has also the character of MLCT/ILCT/LLCT. For 2, the low-lying absorptions at 483 and 484 nm are

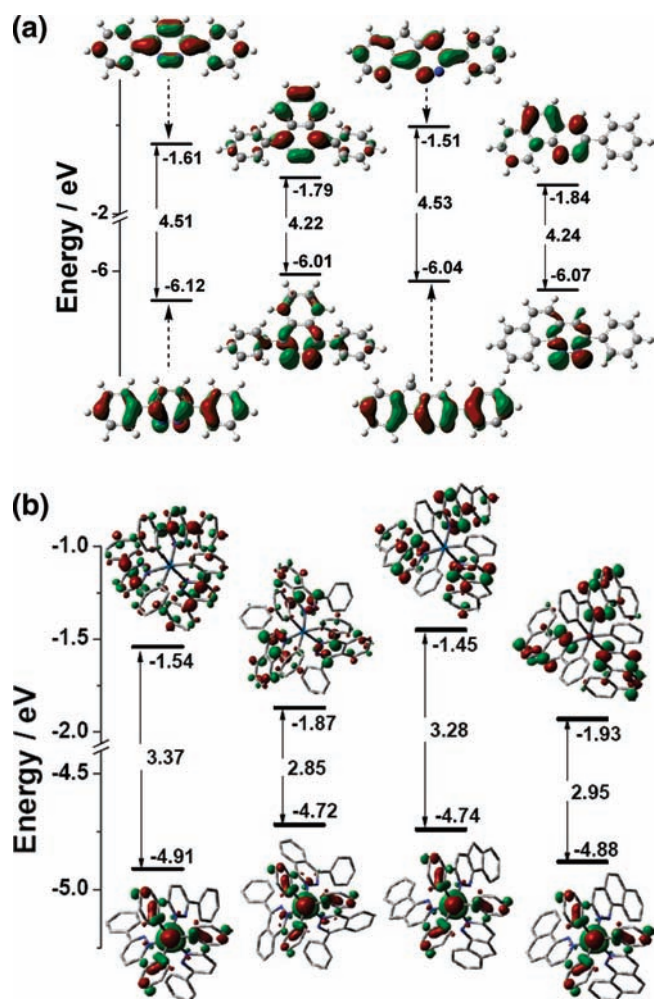


Figure 3. Contour plots of HOMO and LUMO (a) for the ligands 1L–4L and (b) for the studied complexes 1–4.

assigned to MLCT/ILCT/LLCT, and its maximum band at 335 nm is ascribed to MLCT/ILCT character.

On the other hand, although the band locations of 1, 3, and 4 are similar, in the higher energy region around 300 nm, the absorption intensity of 4 is significantly stronger than that of 1 and 3 (Table 3 and Figure 4), while in the lower energy region around 400 nm, the intensities of 1, 3, and 4 are comparable. The large absorption intensities would increase the probability of intersystem crossing (ISC) from singlet to triplet states and hence the possibility to increase the phosphorescent quantum yield.

3.4. Phosphorescence in CH_2Cl_2 Media. The calculated emission energies, transition nature, and the available experimental values are listed in Table 4. The calculated emission energies for 1 (2.03 eV, 610 nm) and 2 (1.85 eV, 672 nm) are slightly smaller as compared to the corresponding experimental values (541 nm¹⁶ and 625 nm¹⁷ for 1 and 2, respectively), but the trend is the same. The emission energy of 1 is similar to that of 3 (2.08 eV), and both complexes have the same phosphorescent characters, that is, metal to one ligand charge transfer and intraligand charge transfer in that ligand. On the other hand, the emission energy of 4 (2.14 eV) is blue-shifted as compared to that of 2 (1.85 eV), but their luminescent nature is nearly the same, that is, metal to three ligands charge transfer and intraligand charge transfer in the three

ligands. The assigned emission characters are consistent with the discussion in section 3.1.

It is unexpected that complex 4 has the shortest wavelength. As compared to the results from the vacuum (Table 5), it is seen that solvent effects have some influence on the calculated emission spectra, in which the values from the vacuum are larger (red-shifted) than those from the solvent, in particular for complexes 2 and 4. The solvent effect makes the spectra blue-shifted 11 nm for 1 and 3, which is 3–4 times smaller than that for 2 and 4 (see Table 5). We guess that the influence of solvent effect on the spectra is related to the distribution of charge transfer, in which the emission spectra of 1 and 3 are dominated by one ligand, but the emission spectra of 2 and 4 are dominated by three ligands. Our calculations also show that 1, 3, and 4 are green-emitters, while 2 is a red-emitter.

Normally, for organic, inorganic, molecular, and polymeric materials, the red shift of absorption and emission spectra can be tuned by the benzannulation of aromatic molecules. However, a previous study indicated that, depending on the site of benzannulation, either red or blue shifts can be observed.³⁰ This is in agreement with our study that the absorption and emission spectra of 4 are blue-shifted as compared to those of 2.

3.5. The PL Quantum Efficiency in CH_2Cl_2 Media. The emission quantum yield (Φ) from an emissive excited state to the ground state is generally formulated as:

$$\Phi = k_r / (k_r + k_{nr}) \quad (1)$$

where k_r and k_{nr} are the radiative and nonradiative rate constants, respectively. Thus, for obtaining an efficient phosphorescent material, a large k_r and a small k_{nr} are required. The rate constants depend strongly on the energy of lowest triplet excited state (E_{T_1}) for phosphorescence, expressed as:

$$k_{nr} = \alpha \exp(-\beta E_{T_1}) \quad (2)$$

$$k_r = \gamma (E_{T_1})^3 |M_{T-S}|^2 \quad (3)$$

where α , β , and γ are constant; $|M_{T-S}|$ is the emission transition moment from the triplet state. Equation 2 is well-known as “the energy gap law”,³¹ which indicates that k_{nr} decreases with the increase of E_{T_1} . In contrary, eq 3 shows that k_r increases with the increase of E_{T_1} . Thus, a large E_{T_1} is essential for an efficient material. Table 4 indicates that 4 has the largest E_{T_1} followed by 3 and 1 in CH_2Cl_2 media. Hence, the assumed complex 4 is a good candidate to be an efficient phosphorescent material.

By use of first-order spin–orbit theory, the $|M_{T-S}|$ can be calculated by the formula:

$$M_{T-S} = \sum_{S_m} \frac{\langle \phi_{T_1} | \hat{H}_{SO} | \phi_{S_m} \rangle}{E_{S_m} - E_{T_1}} \times \langle \phi_{S_m} | e\vec{r}^- | \phi_{S_0} \rangle \quad (4)$$

where \hat{H}_{SO} is the spin–orbit coupling operator. ϕ is the wave function of the corresponding state. E_{S_m} is the energy of the m th singlet excited state (S_m), and $e\vec{r}^-$ is the electric dipole operator. $\langle \phi_{S_m} | e\vec{r}^- | \phi_{S_0} \rangle = (f_{S_m} / (E_{S_m}))^{1/2}$, where f_{S_m} is the oscillator strength of the transition $S_0 \rightarrow S_m$ in absorption spectra. The spin–orbit coupling (SOC) effects are elucidated mainly from the following two aspects. One is the contribution of MLCT in the T_1 state.³² The direct involvement of the d(Ir) orbital enhances the first-order SOC in the $T_1 \rightarrow S_0$ transition, which would result in a drastic decrease of the radiative lifetime and avoid the nonradiative process.³³ Thus, a large MLCT contribution is beneficial to increasing the quantum yield. Table 6 shows

Table 3. Selected Calculated Wavelength (nm)/Energies (eV), Oscillator Strength (*f*), Major Contribution, Transition Characters, and the Experimental Wavelength (nm) for 1–4 in CH₂Cl₂ Media

	state	λ/E	<i>f</i>	configuration	nature	exp.	
1	S ₁	449/2.76	0.020	H→L (0.54)	MLCT/ILCT		
				H→L+1 (0.43)	MLCT/ILCT		
	S ₁₂	399/3.11	0.063	H-2→L+2 (0.39)	MLCT/LLCT/ILCT	400	
				H-1→L+3 (0.39)	MLCT/LLCT/ILCT		
	S ₁₃	399/3.11	0.063	H-2→L+3 (0.39)	MLCT/LLCT/ILCT		
				H-1→L+2 (0.40)	MLCT/LLCT/ILCT		
	S ₃₁	306/4.05	0.378	H-6→L+1 (0.30)	MLCT	284	
				H-5→L (0.43)	MLCT/ILCT		
	2	S ₁	534/2.32	0.030	H→L (0.69)	MLCT/ILCT	
		S ₄	484/2.56	0.079	H-1→L (0.66)	MLCT/ILCT/LLCT	
S ₅		483/2.57	0.080	H-2→L (0.66)	MLCT/ILCT/LLCT		
S ₂₈		335/3.70	0.448	H-6→L (0.54)	MLCT	316	
				H-5→L (0.33)	MLCT/ILCT		
3	S ₁	443/2.80	0.000	H→L+3 (0.66)	MLCT/ILCT		
	S ₂	437/2.84	0.081	H→L (0.67)	MLCT/ILCT		
	S ₉	406/3.05	0.073	H-1→L+3 (0.58)	MLCT/ILCT/LLCT		
	S ₁₀	406/3.05	0.075	H-2→L+3 (0.58)	MLCT/ILCT/LLCT		
	S ₁₆	391/3.17	0.098	H-2→L+5 (0.42)	MLCT/ILCT		
				H-1→L+4 (0.43)	MLCT/ILCT		
	S ₁₇	391/3.17	0.102	H-2→L+4 (0.43)	MLCT/LLCT/ILCT		
				H-1→L+5 (0.43)	MLCT/LLCT		
	S ₂₇	308/4.02	0.303	H-6→L (0.28)	MLCT		
				H-6→L+3 (0.26)	MLCT		
				H-4→L+1 (0.27)	MLCT/ILCT		
				H-4→L+2 (0.23)	MLCT/LLCT		
				H-3→L+2 (0.26)	MLCT/ILCT		
	S ₃₀	306/4.05	0.256	H-5→L (0.61)	ILCT/MLCT		
	S ₃₇	298/4.16	0.303	H-6→L+3 (0.35)	MLCT		
				H-5→L+3 (0.39)	ILCT/MLCT		
4	S ₁	501/2.47	0.012	H→L (0.67)	MLCT/ILCT		
	S ₄	476/2.61	0.035	H-1→L (0.66)	MLCT/ILCT/LLCT		
	S ₅	476/2.61	0.035	H-2→L (0.66)	MLCT/ILCT/LLCT		
	S ₁₃	405/3.06	0.075	H-1→L+3 (0.59)	MLCT/ILCT/LLCT		
	S ₁₄	405/3.06	0.075	H-2→L+3 (0.59)	MLCT/ILCT/LLCT		
	S ₁₈	385/3.22	0.144	H-2→L+5 (0.38)	MLCT/ILCT		
				H-1→L+4 (0.38)	MLCT/LLCT/ILCT		
		S ₅₅	300/4.14	1.729	H-5→L+3 (0.30)	ILCT/MLCT	
					H-4→L+4 (0.23)	MLCT/LLCT/ILCT	
					H-3→L+5 (0.24)	MLCT/LLCT/ILCT	

that the contribution of MLCT is calculated to be 42.2%, 48.1%, 43.9%, and 48.0% for 1–4, respectively. The relatively large MLCT contribution is observed in 2 and 4. The other is the S₁–T₁ energy gap (ΔE_{ST}).²³ According to eq 4, transition moment may partially depend on the ΔE_{ST} . Moreover, the S₁→T₁ ISC due to SOC interactions of the triplet state with singlet state plays an important role in phosphorescent process. The minimal ΔE_{ST} is good for enhancing the transition moment and ISC rate, leading to the increased k_r . The calculated ΔE_{ST} values (Table 6) indicate that 4 has the smallest ΔE_{ST} (0.15 eV), while the other three complexes have quite similar and relatively large values. A large value of $\langle\phi_{S_m}|e\vec{r}|\phi_{S_0}\rangle$ will make $|M_{T-S}|$ and k_r increase. As mentioned earlier, because the absorption band locations of 1, 3, and 4 are similar, and the oscillator strength of 4

is stronger than that of 1 and 3, the value of $\langle\phi_{S_m}|e\vec{r}|\phi_{S_0}\rangle = ((f_{S_m})/(E_{S_m}))^{1/2}$ for 4 could be larger than that for 1 and 3.

In the S₁→T₁ process, the nonradiative geometry relaxation of 4 is also the smallest, because of its smallest absolute ΔBLA (T₁–S₀) values (Table 2) and the smallest Stokes shift (0.33 eV) (Table 6). From the above discussion, we can conclude that the assumed complex 4 is the most efficient green-emitting phosphorescent material among the studied complexes, and the performance of 3 is comparable to that of 1.

3.6. Comparison of Performance in OLEDs. Ionization potential (IP), electron affinity (EA), and migration of charge are the three key factors for designing optoelectronic materials. The charge injection properties of luminescent materials can be evaluated by the EA and IP, which are also closely

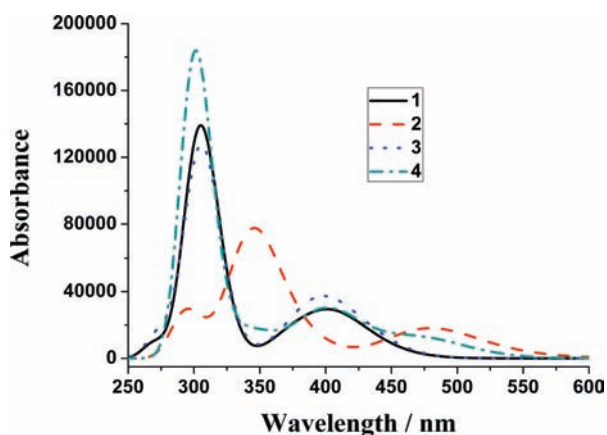
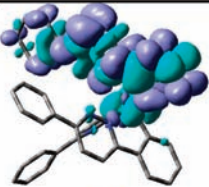

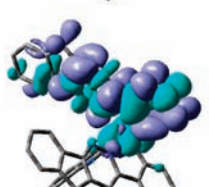
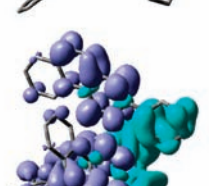


Figure 4. Simulated absorption spectra in CH_2Cl_2 media for complexes 1–4.

Table 4. Calculated Emission Energies of T_1 and Their Transition Nature for Ir(III) Complexes in CH_2Cl_2 Media, as well as the Available Experimental Wavelengths (nm)^a

	$\lambda(\text{nm})/E(\text{eV})$	Nature ^a	Exp.
1	610 / 2.03	 MLCT/IL	541 ¹⁶
2	672 / 1.85	 MLCT/IL	625 ¹⁷
3	596 / 2.08	 MLCT/IL	
4	579 / 2.14	 MLCT/IL	

^a Change of electron density distribution upon the $T_1 \rightarrow S_0$ transition for the studied complexes. Cyan and violet colors represent the decrease and increase of electron density, respectively.

relative to the HOMO and LUMO, respectively.^{25,34} A larger EA (smaller IP) suggests that it is easier to inject electrons (holes) into the emitting materials from the electron (hole)

Table 5. Calculated Emission Wavelength (nm) in a Vacuum and CH_2Cl_2 Media, and Their Differences Δ (nm) for the Studied Ir(III) Complexes

	vacuum	CH_2Cl_2	Δ
1	621	610	11
2	703	672	31
3	607	596	11
4	623	579	44

Table 6. Contribution of MLCT in the T_1 State, TD-DFT Calculated Values of the S_1-T_1 Energy Gaps (ΔE_{ST}), and the Stokes Shifts in Complexes 1–4

	MLCT, %	ΔE_{ST} , eV	Stokes shifts, eV
1	42.2	0.26	0.73
2	48.1	0.25	0.47
3	43.9	0.26	0.72
4	48.0	0.15	0.33

Table 7. Ionization Potentials, Electron Affinities, Extraction Potentials, and Inner Reorganization Energies for Electron/Hole (λ_e/λ_h), in electronvolts

	IP_v	IP_a	HEP	EA_v	EA_a	EEP	λ_e	λ_h
1	5.93	5.85	5.74	0.52	0.62	0.78	0.26	0.19
2	5.68	5.58	5.39	0.85	1.00	1.08	0.23	0.29
3	5.74	5.66	5.55	0.48	0.54	0.59	0.11	0.19
4	5.83	5.75	5.54	0.93	1.03	1.13	0.2	0.29

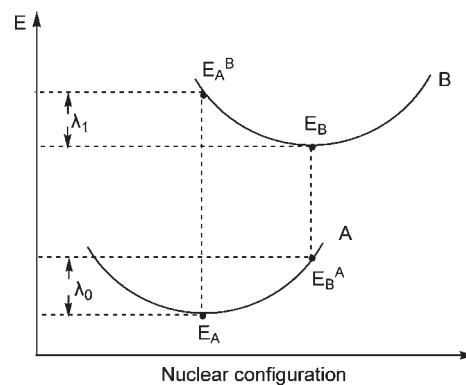


Figure 5. Schematic description of the inner reorganization energy.

transporting layer. The calculated vertical IP (IP_v), adiabatic IP (IP_a), vertical EA (EA_v), and adiabatic EA (EA_a) are listed in Table 7. It shows that 3 and 4 have smaller IP values and large hole injection abilities as compared to 1. Complex 2 has the smallest IP value, which is consistent with its highest HOMO energy level, and thus its hole injection is the easiest. Corresponding to the lowest LUMO energy level, the assumed complex 4 has large EA value and enhanced electron injection ability as compared to the experimentally obtained complexes 1 and 2.

According to the semiclassical Marcus theory,³⁵ the rate of intermolecular charge (hole and electron) transfer (K_{et}) can be

estimated by the following formula:

$$K_{\text{et}} = A \exp(-\lambda/4k_{\text{B}}T) \quad (5)$$

where λ is the reorganization energy, A is a prefactor related to the electronic coupling between adjacent molecules, and T and k_{B} are the temperature and Boltzmann constant, respectively. As previously reported, due to the limited intermolecular charge transfer range in solid state, the mobility of charges dominantly relates to the reorganization energy λ for OLEDs materials.^{36,37} Therefore, at constant temperature, the low λ value is necessary for an efficient charge transport process. Herein, any environmental influence is ignored, and we focus on the inner reorganization energy λ_{i} , which is caused by the change of the internal nuclear coordinates from the reactant A to the product B and vice versa (Figure 5). It can be evaluated as the sum of two relaxation energies according to the following formula:

$$\lambda_{\text{i}} = \lambda_0 + \lambda_1 = (E_{\text{B}}^{\text{A}} - E_{\text{A}}) + (E_{\text{A}}^{\text{B}} - E_{\text{B}}) \quad (6)$$

where E_{A} and E_{A}^{B} are the energies of A and B at the optimized geometry of A, respectively; E_{B}^{A} and E_{B} are the energies of A and B at the optimized geometry of B, respectively. Figure 5 shows that the reorganization energy for hole transport $\lambda_{\text{h}} = \text{IP}_{\text{v}} - \text{HEP}$. HEP represents hole extraction potential, which is the energy difference between M (neutral molecule) and M^+ (cationic), using M^+ geometry. Similarly, the reorganization energy for electron transport $\lambda_{\text{e}} = \text{EEP} - \text{EA}_{\text{v}}$. EEP represents electron extraction potential, which is the energy difference between M and M^- (anionic), using M^- geometry.

The inner reorganization energies (Table 7) indicate that the differences between λ_{h} and λ_{e} for **1–4** are small, so hole and electron transfer balance could be achieved easily in emitting layer, which is the key factor for materials used in OLEDs. Moreover, the λ_{e} values of the assumed complexes **3** and **4** are smaller than those of complexes **1** and **2**, leading to the easier electron transfer for **3** and **4**.

4. CONCLUSIONS

We have investigated the optoelectronic properties of homoleptic Ir(III) complexes with $\text{C}^{\wedge}\text{N}=\text{N}$ ligands by using the density functional method. The study indicates that the assumed complex **4** may have the smallest nonradiative rate constant and largest radiative rate constant, which leads to its highest photoluminescent quantum efficiency among the studied complexes. Thus, **4** instead of the experimentally found complex **1** could become the potential candidate for efficient green-emitting material. Moreover, **4** has the smallest structural relaxation between the lowest triplet state and the ground state and the smallest Stokes shift in solvent (CH_2Cl_2 media). The photophysical properties of the assumed complex **3** can be comparable to that of **1**. For **1** and **3**, their emission energies are nearly the same. Their emission characters are also similar and mainly dominated by one ligand. However, for **2** and **4**, the emission energy of **4** is largely blue-shifted as compared to that of **2**, but their luminescent nature is nearly the same and dominated by the three ligands. Moreover, it is found that the influence of solvent effect on spectra is related to the extension of charge transfer.

■ ASSOCIATED CONTENT

Supporting Information. Cartesian coordinates of the four studied complexes from B3LYP-optimized geometries. This material is available free of charge via the Internet at <http://pubs.acs.org>.

■ AUTHOR INFORMATION

Corresponding Author

*E-mail: zjwu@ciac.jl.cn.

■ ACKNOWLEDGMENT

We thank the National Natural Science Foundation of China (NSFC) for financial support (Grant Nos. 90922015, 20831004) and NSFC Fund for Creative Research Group (20921002).

■ REFERENCES

- Reineke, S.; Lindner, F.; Schwartz, G.; Seidler, N.; Walzer, K.; Lussem, B.; Leo, K. *Nature* **2009**, *459*, 234.
- Chiu, Y. C.; Hung, J. Y.; Chi, Y.; Chen, C. C.; Chang, C. H.; Wu, C. C.; Cheng, Y. M.; Yu, Y. C.; Lee, G. H.; Chou, P. T. *Adv. Mater.* **2009**, *21*, 2221.
- Ikai, M.; Tokito, S.; Sakamoto, Y.; Suzuki, T.; Taga, Y. *Appl. Phys. Lett.* **2001**, *79*, 156.
- Adachi, C.; Baldo, M. A.; Thompson, M. E.; Forrest, S. R. *J. Appl. Phys.* **2001**, *90*, 5048.
- Baldo, M. A.; O'Brien, D. F.; You, Y.; Shoustikov, A.; Sibley, S.; Thompson, M. E.; Forrest, S. R. *Nature* **1998**, *395*, 151.
- Lamansky, S.; Djurovich, P.; Murphy, D.; Abdel-Razzaq, F.; Lee, H. E.; Adachi, C.; Burrows, P. E.; Forrest, S. R.; Thompson, M. E. *J. Am. Chem. Soc.* **2001**, *123*, 4304.
- Chen, Z. Q.; Bian, Z. Q.; Huang, C. H. *Adv. Mater.* **2010**, *22*, 1534.
- Jiang, C. Y.; Yang, W.; Peng, J. B.; Xiao, S.; Cao, Y. *Adv. Mater.* **2004**, *16*, 537.
- Baldo, M. A.; Adachi, C.; Forrest, S. R. *Phys. Rev. B* **2000**, *62*, 10967.
- Reineke, S.; Walzer, K.; Leo, K. *Phys. Rev. B* **2007**, *75*, 125328.
- Staroske, W.; Pfeiffer, M.; Leo, K.; Hoffmann, M. *Phys. Rev. Lett.* **2007**, *98*, 197402.
- Chen, K.; Yang, C. H.; Chi, Y.; Liu, C. S.; Chang, C. H.; Chen, C. C.; Wu, C. C.; Chung, M. W.; Cheng, Y. M.; Lee, G. H.; Chou, P. T. *Chem.-Eur. J.* **2010**, *16*, 4315.
- Adachi, C.; Baldo, M. A.; Forrest, S. R.; Lamansky, S.; Thompson, M. E.; Kwong, R. C. *Appl. Phys. Lett.* **2001**, *78*, 1622.
- Takizawa, S.; Nishida, J.; Tsuzuki, T.; Tokito, S.; Yamashita, Y. *Inorg. Chem.* **2007**, *46*, 4308.
- Lamansky, S.; Djurovich, P.; Murphy, D.; Abdel-Razzaq, F.; Kwong, R.; Tsyba, I.; Bortz, M.; Mui, B.; Bau, R.; Thompson, M. E. *Inorg. Chem.* **2001**, *40*, 1704.
- Gao, Z. Q.; Mi, B. X.; Tam, H. L.; Cheah, K. W.; Chen, C. H.; Wong, M. S.; Lee, S. T.; Lee, C. S. *Adv. Mater.* **2008**, *20*, 774.
- Mi, B. X.; Wang, P. F.; Gao, Z. Q.; Lee, C. S.; Lee, S. T.; Hong, H. L.; Chen, X. M.; Wong, M. S.; Xia, P. F.; Cheah, K. W.; Chen, C. H.; Huang, W. *Adv. Mater.* **2009**, *21*, 339.
- Tong, B. H.; Mei, Q. B.; Wang, S. J.; Fang, Y.; Meng, Y. Z.; Wang, B. J. *Mater. Chem.* **2008**, *18*, 1636.
- Becke, A. D. *J. Chem. Phys.* **1993**, *98*, 5648.
- Lee, C. T.; Yang, W. T.; Parr, R. G. *Phys. Rev. B* **1988**, *37*, 785.
- Hay, P. J.; Wadt, W. R. *J. Chem. Phys.* **1985**, *82*, 270.
- Hay, P. J.; Wadt, W. R. *J. Chem. Phys.* **1985**, *82*, 299.
- Avilov, I.; Minoofar, P.; Cornil, J.; De Cola, L. *J. Am. Chem. Soc.* **2007**, *129*, 8247.
- Li, X. N.; Wu, Z. J.; Si, Z. J.; Zhang, H. J.; Zhou, L.; Liu, X. J. *Inorg. Chem.* **2009**, *48*, 7740.
- Shi, L. L.; Geng, Y.; Gao, H. Z.; Su, Z. M.; Wu, Z. J. *Dalton Trans.* **2010**, *39*, 7733.
- Frisch, M. J.; Trucks, G. W.; Schlegel, H. B.; Scuseria, G. E.; Robb, M. A.; Cheeseman, J. R.; Montgomery, J. A., Jr.; Vreven, T.; Kudin, K. N.; Burant, J. C.; Millam, J. M.; Iyengar, S. S.; Tomasi, J.; Barone, V.; Mennucci, B.; Cossi, M.; Scalmani, G.; Rega, N.; Petersson, G. A.; Nakatsuji, H.; Hada, M.; Ehara, M.; Toyota, K.; Fukuda, R.

Hasegawa, J.; Ishida, M.; Nakajima, T.; Honda, Y.; Kitao, O.; Nakai, H.; Klene, M.; Li, X.; Knox, J. E.; Hratchian, H. P.; Cross, J. B.; Adamo, C.; Jaramillo, J.; Gomperts, R.; Stratmann, R. E.; Yazyev, O.; Austin, A. J.; Cammi, R.; Pomelli, C.; Ochterski, J. W.; Ayala, P. Y.; Morokuma, K.; Voth, G. A.; Salvador, P.; Dannenberg, J. J.; Zakrzewski, V. G.; Dapprich, S.; Daniels, A. D.; Strain, M. C.; Farkas, O.; Malick, D. K.; Rabuck, A. D.; Raghavachari, K.; Foresman, J. B.; Ortiz, J. V.; Cui, Q.; Baboul, A. G.; Clifford, S.; Cioslowski, J.; Stefanov, B. B.; Liu, G.; Liashenko, A.; Piskorz, P.; Komaromi, I.; Martin, R. L.; Fox, D. J.; Keith, T.; Al-Laham, M. A.; Peng, C. Y.; Nanayakkara, A.; Challacombe, M.; Gill, P. M. W.; Johnson, B.; Chen, W.; Wong, M. W.; Gonzalez, C.; Pople, J. A. *Gaussian 03*, revision C.02; Gaussian, Inc.: Pittsburgh, PA, 2004.

(27) Li, X. N.; Wu, Z. J.; Liu, X. J.; Zhang, H. J. *J. Phys. Chem. A* **2010**, *114*, 9300.

(28) Shi, L. L.; Li, T.; Zhao, S. S.; Li, H.; Su, Z. M. *Theor. Chem. Acc.* **2009**, *124*, 29.

(29) Casado, J.; Quirante, J. J.; Hernandez, V.; Navarrete, J. T. L.; Takimiya, K.; Otsubo, T. *J. Phys. Chem. B* **2004**, *108*, 7611.

(30) Hanson, K.; Roskop, L.; Djurovich, P. I.; Zahariev, F.; Gordon, M. S.; Thompson, M. E. *J. Am. Chem. Soc.* **2010**, *132*, 16247.

(31) Wilson, J. S.; Chawdhury, N.; Al-Mandhary, M. R. A.; Younus, M.; Khan, M. S.; Raithby, P. R.; Kohler, A.; Friend, R. H. *J. Am. Chem. Soc.* **2001**, *123*, 9412.

(32) Li, J.; Djurovich, P. I.; Alleyne, B. D.; Yousufuddin, M.; Ho, N. N.; Thomas, J. C.; Peters, J. C.; Bau, R.; Thompson, M. E. *Inorg. Chem.* **2005**, *44*, 1713.

(33) Yang, C. H.; Cheng, Y. M.; Chi, Y.; Hsu, C. J.; Fang, F. C.; Wong, K. T.; Chou, P. T.; Chang, C. H.; Tsai, M. H.; Wu, C. C. *Angew. Chem., Int. Ed.* **2007**, *46*, 2418.

(34) Shi, L. L.; Liao, Y.; Yang, G. C.; Su, Z. M.; Zhao, S. S. *Inorg. Chem.* **2008**, *47*, 2347.

(35) Marcus, R. A. *Rev. Mod. Phys.* **1993**, *65*, 599.

(36) Hush, N. S. *J. Chem. Phys.* **1958**, *28*, 962.

(37) Marcus, R. A. *J. Chem. Phys.* **1956**, *24*, 966.